Chemical reactivity of supported gold. A structural study by small-angle X-ray scattering and x-ray absorption spectroscopy

ARTICLE *in* THE JOURNAL OF PHYSICAL CHEMISTRY · SEPTEMBER 1979

Impact Factor: 2.78 · DOI: 10.1021/j100482a022

8 AUTHORS, INCLUDING:

Stefano Enzo
Università degli Studi di Sassari
236 PUBLICATIONS **2,788** CITATIONS
SEE PROFILE

Gilberto Vlaic
Sincrotrone Trieste S.C.p.A.
83 PUBLICATIONS **2,011** CITATIONS
SEE PROFILE

Signorino Galvagno
Università degli Studi di Messina
184 PUBLICATIONS **4,578** CITATIONS
SEE PROFILE

in cation solvation upon the formation of the activated complex. This observation also indicates that benzene as a solvent does not interact strongly with the ion pair complexes.

Acknowledgment. This research was supported by the Robert A. Welch Foundation of Houston, Texas, and by the National Aeronautics and Space Administration Grant NSG-1316.

References and Notes

(1) F. DeBoer and E. L. Mackor, *Proc. Chem. Soc.*, 23 (1963); *J. Am. Chem. Soc.*, **86**, 1513 (1964).
(2) J. H. Sharp and M. C. Symons, "Ions and Ion Pairs in Organic Reactions", Vol. 1, M. Swarc, Ed., Wiley-Interscience, New York, 1972.
(3) P. S. Gill and T. E. Gough, *Can. J. Chem.*, **45**, 2112 (1967).
(4) M. P. Khakhar, B. S. Prabhananda, and M. R. Das, *J. Am. Chem. Soc.*, **89**, 100 (1967).
(5) P. S. Gill and T. E. Gough, *Trans. Faraday Soc.*, **64**, 1997 (1968).
(6) J. Oakes and M. C. R. Symons, *Trans. Faraday Soc.*, **66**, 10 (1970).
(7) T. E. Gough and P. R. Hindle, *Can. J. Chem.*, **49**, 2412 (1971).
(8) G. F. Pedulli, P. Zanirato, A. Alberti, M. Guerra, and M. Tiecco, *J. Chem. Soc., Perkin Trans. 2*, 946 (1976).
(9) K. S. Chen and N. Hirota, *J. Phys. Chem.*, **82**, 1133 (1978).
(10) B. Kaempf, S. Raynal, A. Collet, F. Schue, S. Bolleau, and J. Lehn, *Angew. Chem., Int. Ed. Engl.*, **13**, 611 (1974).
(11) M. A. Komarynsky and S. I. Weissman, *J. Am. Chem. Soc.*, **97**, 1589 (1975).
(12) M. P. Eastman, D. A. Ramirez, C. D. Jaeger, and M. T. Watts, *J. Phys. Chem.*, **80**, 1928 (1977).
(13) M. P. Eastman, Y. Chiang, G. V. Bruno, and C. A. McGuyer, *J. Phys. Chem.*, **81**, 1928 (1977).
(14) G. V. Bruno, J. K. Harrington, and M. P. Eastman, *J. Phys. Chem.*, **81**, 1111 (1977).
(15) G. K. Fraenkel, *J. Phys. Chem.*, **71**, 139 (1967).
(16) J. A. Pople, W. G. Schneider, and H. J. Bernstein, "High Resolution Nuclear Magnetic Resonance", McGraw-Hill, New York, 1959.
(17) M. T. Watts, M. Lu, and M. P. Eastman, *J. Phys. Chem.*, **77**, 825 (1973).
(18) K. H. Wong, T. Konlzer, and J. Smid, *J. Am. Chem. Soc.*, **92**, 666 (1970).
(19) U. Takaki, T. E. Hogen Esch, and J. Smid, *J. Am. Chem. Soc.*, **93**, 6760 (1971).
(20) U. Takaki, T. E. Hogen Esch, and J. Smid, *J. Phys. Chem.*, **76**, 2152 (1972).
(21) C. J. Pedersen and H. K. Frensdorff, *Angew. Chem., Int. Ed. Engl.*, **11**, 16 (1972).

Chemical Reactivity of Supported Gold. A Structural Study by Small-Angle X-ray Scattering and X-ray Absorption Spectroscopy

G. Cocco, S. Enzo, G. Fagherazzi,* L. Schiffini,

Istituto di Chimica Fisica dell'Università di Venezia, Dorso Duro 2137, I-30123 Venezia, Italy

I. W. Bassi,† G. Vlaic,

Istituto Donegani, I-28100 Novara, Italy

S. Galvagno,‡ and G. Parravano§

Department of Chemical Engineering, University of Michigan, Ann Arbor, Michigan 48109 *(Received August 3, 1978; Revised Manuscript Received March 12, 1979)*

Publication costs assisted by Istituto di Chimica Fisica dell' Università di Venezia

Preparations of Au supported on SiO_2 and Al_2O_3 were characterized by small-angle X-ray scattering (SAXS), wide-angle X-ray scattering (WAXS), extended X-ray absorption fine structure spectroscopy (EXAFS), and transmission electron microscopy (TEM). The L_{III} X-ray absorption coefficient was used in the EXAFS analysis and the radial structure function was calculated. The interatomic distances and coordination numbers of Au preparations were obtained. EXAFS data indicated an interaction between Au and Al_2O_3, while no evidence of interaction between gold and SiO_2 could be detected. The average Au–Au coordination number was also determined on the basis of particle diameters measured by SAXS and WAXS. Percentages of total Au present in the metallic phase, directly determined by EXAFS, were compared with the ones computed on the basis of SAXS and WAXS particle size measurements. By SAXS measurements normal-logarithmic particle size distribution curves and metal surface area were obtained. From the particle size and Au concentrations so determined the percentage of Au exposed was calculated. The catalytic activity of the three catalysts examined was studied for the isotopic equilibration reaction $H_2(g) + D_2(g) \rightarrow 2HD(g)$, and for the reduction of NO by H_2. Moreover, selectivity measurements are reported for the reduction of NO to N_2. An interpretation of possible relationships among catalytic activity, selectivity, degree of dispersion of metal, and interaction between gold and support material is discussed.

Introduction

Finely divided Au imbedded in ceramic supports acquires a degree of chemical reactivity unmatched by more massive forms of the metal including thin films. Several reactions involving hydrogen and oxygen transfer were found to be catalyzed by supported Au under relatively mild conditions of pressure and temperature. The reactivity of supported Au surfaces toward gas phase molecules is paralleled by that with the supporting material. In fact, chemical interactions between Au and the support extended to various supports modifying, in a characteristic fashion, the reaction selectivity in the reduction of NO by H_2.[1] A fundamental question in the

† Deceased April 9, 1979.
‡ On leave from the Donegani Research Institute, Montedison S.p.A., Novara, Italy.
§ Deceased April 1, 1978.

0022-3654/79/2083-2527$01.00/0

TABLE I: Supported Au Samples

sample	support	Au,[d] wt %	prep method
A1141	η-Al_2O_3	6.9	*a*
4433	SiO_2	2.2	*b*
2441b	SiO_2	3.2	*c*

[a] Impregnation with $HAuCl_4$, reduction with oxalic acid, 2 h, 350 °C, 1 mmHg. [b] Cationic exchange with $[Au(en)_2]Cl_3$, 2 h, 400 °C in H_2. [c] Impregnation with $KAu(CN)_2$, 2 h, 350 °C, 0.1 mmHg. [d] By atomic absorption and neutron activation analysis: the first method gives a precision of ±10% and the second one ±5%.

genesis and control of supported Au reactivity is the role of morphological factors of the Au "particle", including shape, size, size distribution, juxtaposition with the support phase, the role of two-dimensional aggregates, and of "dissolution" into the support vs. dispersion on the support. Inextricably related to these potential morphological factors are the electronic conditions at the Au surface reactive site, namely, the density and energy of uppermost filled electron states, their orbital symmetry, and correct location above surface atoms or above surface positions between atoms. For the correct theoretical treatment of the reactivity of gold surfaces the above information is necessary.

To further progress in this direction we felt that an in depth analysis of typical supported gold preparations by a combination of X-ray absorption spectroscopy and X-ray scattering might prove useful and might contribute to a better understanding of the above factors, their genesis, and their role in gold reactivity. Because of the need to cover initially morphological factors in three- and two-dimensional aggregates and structural and electron binding conditions in isolated Au atoms, a combination of wide-angle X-ray scattering (WAXS), small-angle X-ray scattering (SAXS), and extended X-ray absorption fine structure spectroscopy (EXAFS) seemed well suited for the problem at hand. In principle, by means of a combination of these structural techniques, it is possible to determine particle size, shape, and total metallic Au content (WAXS), metal surface area, particle size distribution as well as metallic Au content (SAXS), the average coordination of Au, Au–Au distance, presence of bonding between Au and other elements (oxygen) and, finally, the average charge on the Au, and, therefore, obtain some indication of its binding energy and the presence of characteristic energy shifts (EXAFS). Furthermore, in order to verify some SAXS and WAXS experimental data, the Au preparations were subjected to transmission electron microscopy (TEM). Finally, the information obtained from the physical and chemical characterization has been applied to the interpretation of the catalytic activity and selectivity of the same supported Au preparations in the reduction of NO by molecular hydrogen.

Experimental Section

Materials. Three samples of supported Au (Table I) were investigated.

A1141. Au on η-Al_2O_3 (Davison, surface area 230 m^2/g) was prepared by Al_2O_3 impregnation with an aqueous solution of $HAuCl_4 \cdot 3H_2O$ (Baker Co.), followed by reduction with 2% oxalic acid solution at 40 °C, filtering, washing, drying, and heating at 350 °C for 2 h, under 0.1 mmHg.

Au 2441b. Au on amorphous SiO_2 (C. Erba, surface area 414 m^2/g) was prepared by SiO_2 impregnation with an aqueous solution of $KAu(CN)_2$, followed by drying first at 100 °C and then at 110 °C in an oven under vacuum, and heating at 350 °C for 2 h, under 0.1 mmHg.

Au 4433. Au on amorphous SiO_2 (C. Erba, surface area 414 m^2/g), pretreated for 150 min at room temperature with an aqueous solution of NH_3 (1:1 concentration), was prepared by ion exchange with an aqueous solution of $[Au(en)_2]Cl_3$ (en = ethylenediamine), followed by drying in an oven under vacuum at 100 °C, and, finally, reducing with flowing hydrogen at 420 °C for 2.5 h.

The materials employed as references for Au were Au foil, $HAuCl_4 \cdot 3H_2O$, and Au_2O_3. The same standards were used in a previous work of ours.[2]

Procedure. A. SAXS Experiments. SAXS experiments were carried out with a Kratky Paar camera aligned following the method already described.[3] The camera was equipped with a vacuum collimation system and a Philips Xe-filled proportional counter with pulse-height discrimination. Front slits of 80 μm were employed and the observed intensities were automatically explored with an electronically programmed step scanner. SAXS curves were measured to high precision by the fixed counting technique (10^5 counts per point). Ni-filtered Cu Kα radiation and a special Philips tube having focus dimensions of 2 × 12 mm were employed. The catalysts as well as the two support materials were homogeneously dispersed inside platelike holders, 0.3 cm, 3.9 cm, 0.05 cm. In order to eliminate interferences due to electron density heterogeneities arising from the micropores present in the Al_2O_3 and SiO_2 particles the pore maskant method[4] was used. For catalyst A1141, CH_2I_2 was employed as the masking liquid, whereas for catalysts 4433 and 2441b, $C_2H_4Br_2$ was used. These liquids have an electron density very close to that of the corresponding support, as it may be seen from Table II. The pore maskant liquids were included inside the pores by impregnation. The best results were obtained by using the same amount of pore maskant liquid for each pair of catalyst and support examined (about 0.25 cm^3/g of η-Al_2O_3 and about 0.35 cm^3/g of SiO_2). The optimum conditions for pore maskant impregnation were found by determining the liquid concentration by weighing, after having found by X-ray absorption measurements that the support was saturated without excess liquid.

The SAXS intensities of the support material treated with the pore maskant were subtracted from the SAXS intensities of the corresponding catalyst under study, after having taken into account the relative attenuation factors. In order to determine the Au particle concentration responsible for the observed SAXS and the Au surface area, we determined the absolute intensities by means of a polyethylene (Lupolen) calibration sample.[5]

TABLE II: Mass and Electronic Densities of Support Materials

sample	support	mass density, g/cm³	electron density,[a] g electron/cm³	pore maskant electron density, g electron/cm³
A1141	η-Al_2O_3	3.25	1.594	1.415 (CH_2I_2)
4433	SiO_2	2.19	1.093	0.998 (CH_2BrCH_2Br)
2441b	SiO_2	2.19	1.093	0.998 (CH_2BrCH_2Br)

[a] Defined by $\Sigma Z_i \rho_m / M$, where Z_i is the number of electrons in the *i*th atom of the compound, ρ_m, the mass density, and M, the molecular weight.

B. EXAFS Experiments. EXAFS experiments were carried out with a conventional X-ray tube with an Ag target, a LiF monochromator, and a scintillation counter. Samples were mounted on the sample holder in a glove bag filled with dry nitrogen; they were then transferred into a steel cell equipped with Mylar windows. The cell was pumped to $\sim 10^{-6}$ mmHg and cooled to liquid nitrogen temperature for the duration of the X-ray absorption measurements.[6,7] A fixed 10^5 counts were counted for each step. Approximately 10 passes through each absorption edge were averaged (from ~600 eV below the edge to ~1200 eV above the edge) to obtain the desired statistics. In spite of the high statistics, the electrical and mechanical instabilities of such a conventional system do not warrant the same ratio between the signal height and the background noise which can be reached when synchrotron light is used as an X-ray source.

The details for the determination of the absorption coefficient, for the background correction, and for the computational procedure have been described elsewhere.[8] The precision of the energy scale was defined on the basis of characteristic and/or impurity lines originated by the X-ray tube silver target, and is of about 40 ppm.[9,10] The AuL_{III} absorption edge was measured for each sample.

C. WAXS Experiments. WAXS experiments were conducted by means of a powder diffractometer equipped with a scintillation counter, a pulse-height analyzer, and a Guinier–Jagodzinski camera.[11] The X-ray diffraction patterns of supported Au preparations showed peaks of both metallic Au and support materials while there was no detectable traces of the starting Au compounds used in the preparation of the catalysts. From the half-peak widths, the average dimensions of the metallic Au crystallites were calculated. Powder diffractometer traces, obtained with a rotating sample holder, were also used to determine the weight percent of metallic Au present in the catalysts by the internal standard method (CaF_2), which measures the integrated intensities of metallic Au reflections with reference to a calibration curve obtained with mixtures of known composition. The X-ray diffraction patterns of the reference materials, Au foil, and $HAuCl_4 \cdot 3H_2O$ were consistent with literature data; however, Au_2O_3 was of dubious crystallinity. Its pattern showed only a trace of broad Au peaks. The problem of crystallization of Au_2O_3 has been discussed previously[12] and the Au–O distance of 2.04 Å found by these authors was assumed for the present Au_2O_3 sample. The Au–O distance in CsAuO is 2.26 Å,[13] while it ranges from 2.40 to 1.87 Å in the tetrameric molecule of dimethylgold(III) hydroxide.[14]

D. TEM. TEM microphotographs were taken on carbon extractive replicas for the three powdered samples after dissolution of the support material with HF solutions. A Philips 300 EM transmission electron microscope was employed.

Results

A. SAXS. Figure 1 shows plots log J vs. h^2 and Figure 2 shows plots log J vs. log h for the three catalysts. J (counts s^{-1}) is the normalized experimental intensity diffused by an "infinite" linear beam and $h = 4\pi \sin\theta/\lambda$ is the reciprocal space variable with 2θ Bragg angle and λ the wavelength of the Cu Kα radiation (1.5418 Å). According to the already described procedures, the curves reported in these figures refer only to the metallic microparticles of Au. From the values of Porod (D_P) as well as Guinier diameters (D_G), obtained following well-known methods for the approximation of spherical metallic particles,[15] it is possible to establish a log-normal particle diameter distribution responsible for the observed SAXS

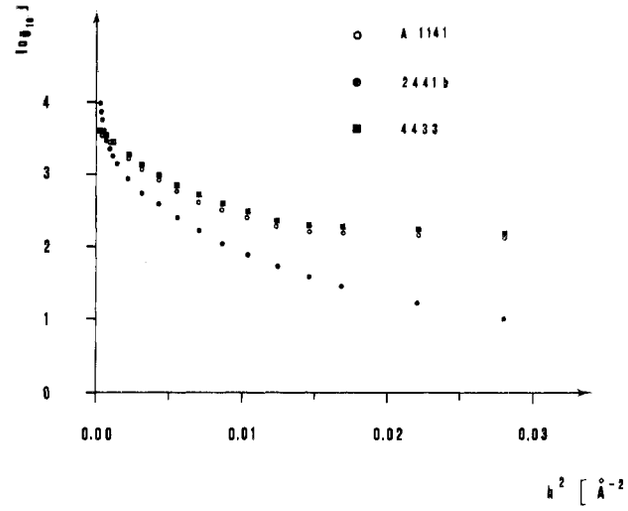

Figure 1. Guinier plots log J vs. h^2 of the three gold-supported catalysts. The SAXS intensity J is referred to gold particles (O) A1141, (●) 2441b, and (■) 4433.

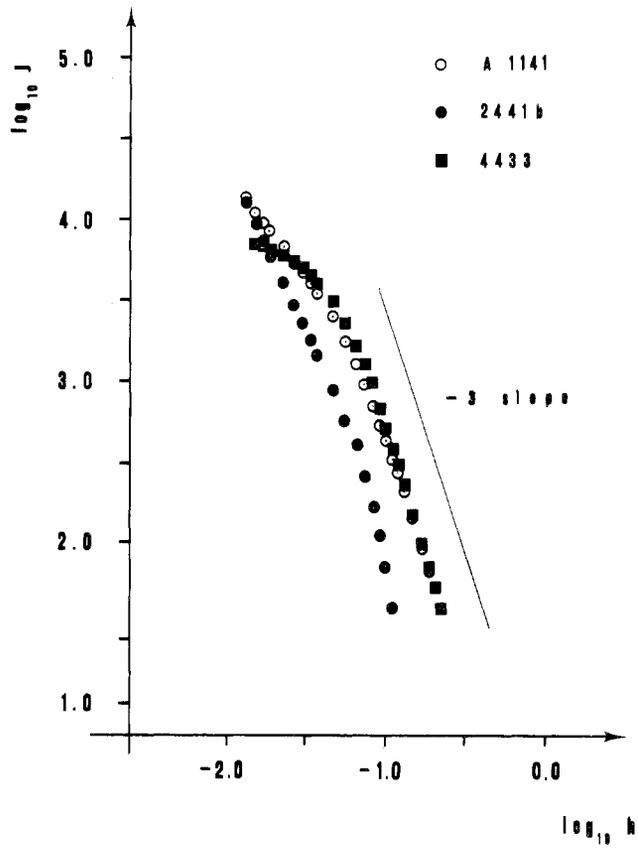

Figure 2. log J vs. log h plots for the three catalysts examined, where the slope −3 is shown. The SAXS intensity J is referred to gold particles (O) A1141, (●) 2441b, and (■) 4433.

curves.[16,17] In fact, D_G can be determined from the square root of the slope of the log J vs. h^2 curve (Figure 1) at small values of h, and D_P can be determined from the expression

$$D_P = \frac{3}{2(1-c)} \frac{\int_0^\infty J(h) h \, dh}{K_h} \qquad (1)$$

where $K_h = \lim_{h\to\infty} h^3 J$ and c is the volume fraction of the Au particles responsible of the observed SAXS. Figure 2 shows the log J vs. log h plots for the three gold supported catalysts, where the slope −3 is shown. The volume fraction

TABLE III: SAXS Characteristics of Supported Au

catalysts	D_G,[a,b] Å	D_P,[a,c] Å	c_{SAXS},[a,d] wt %	S_{sp},[a,e,f] m^2/g of metal
A1141	64	44	1.8	72
4433	76	40	2.0	77
2441b	229	162	3.0	19

[a] The measurement precision for these parameters is ±20%. [b] Guinier diameter. [c] Porod diameter. [d] Metal concentration. [e] Metal surface area. [f] This value is calculated from the corresponding c_{SAXS} value.

of the Au particles was directly obtained by X rays with the following relationship:[18]

$$c(1-c) = \frac{\int_0^\infty J(m)m\,dm}{(16.73 \times 10^{-3})72.2 J_N a^2 \Delta\rho^2 t} \quad (2)$$

where m is the distance (in cm) on the recording plane between the primary and the diffracted ray, 72.2 is a constant for the Lupolen calibration sample which takes into account also the attenuation factor; J_N is the intensity scattered from the calibration sample (counts s^{-1}) at the Bragg angle 2θ corresponding to 150 Å; a is the distance (in cm) between the sample and the recording plane; $\Delta\rho^2$ is the square of the electron density difference between Au particles and matrix in a biphase model hypothesis;[17] t is the thickness (in cm) of the sample under examination. By using a log-normal diameter distribution, the moments of the variable D, i.e., D^g, are log-normally distributed, we can determine the average value of the gth moment by

$$\langle D^g \rangle = \int_0^\infty D^g\, P(D)\, dD \quad (3)$$

where $P(D)$ is the log-normal distribution function given by:

$$P(D) = \frac{1}{(2\pi)^{1/2} D \ln \sigma} \exp\left[-\left(\frac{\ln D - \ln \mu}{2^{1/2} \ln \sigma}\right)^2\right] \quad (4)$$

with μ the geometric mean of the distribution and σ the square root of the variance of the distribution. From eq 3 and 4

$$\langle D^g \rangle = \exp\left(g \ln \mu + \frac{g^2}{2} \ln^2 \sigma\right) \quad (5)$$

For spherical particles, D_G and D_P become ratios of moments of the size distribution,[16] namely

$$D_G = [\langle D^7 \rangle / \langle D^5 \rangle]^{1/2} \quad (6)$$

$$D_P = \langle D^3 \rangle / \langle D^2 \rangle \quad (7)$$

Substituting eq 6 and 7 into eq 5, we obtained the following expressions for D_G and D_P:

$$D_G = \exp(\ln \mu + 6 \ln^2 \sigma) \quad (8)$$

$$D_P = \exp(\ln \mu + 2.5 \ln^2 \sigma) \quad (9)$$

From eq 8 and 9, the parameters μ and σ may be calculated.[17] Using absolute intensities and Kratky's formalism,[18] we computed the metal surface area, S_{sp}, as follows:

$$S_{sp} = \frac{9.74 \times 10^6 K_m}{a^3 (72.2) J_N \Delta\rho^2 t d_b} \ (m^2/g \text{ of metal}) \quad (10)$$

where $K_m = \lim_{m\to\infty} m^3 J$ and d_b is the Au mass density calculated from the c value. The computed values of D_G, D_P, c_{SAXS} (now expressed in weight percent), and S_{sp} are reported in Table III for the three supported Au catalysts,

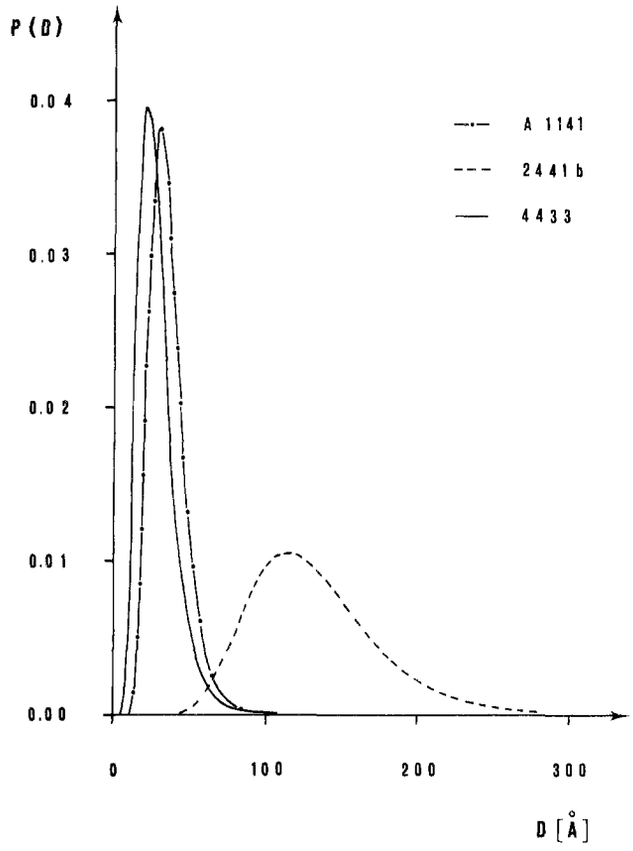

Figure 3. Gold particles log normal size distributions for the three catalysts determined by SAXS methods: (-·-) A1141, (---) 2441b, (—) 4433.

whereas the relative metal particle diameters distributions are shown in Figure 3. It is worth noting that, for sample A1141, the value of c_{SAXS} is not in good agreement with the analytical value reported in Table I. As will be discussed later this is due partly to the presence in this sample of Au particles larger than those observable within the SAXS experimental limits (~1000–1500 Å), and partly to the presence of small Au aggregates or Au atomically dispersed inside the spinel η-Al_2O_3 structure. A precise error analysis of SAXS parameters is possible only by means of several repeated tests, nevertheless the procedures described here are claimed to give Porod and Guinier diameters as well as metal surface area and metal concentration with a precision of ±20% for a related series of samples.[19] This precision was confirmed also in our case by some repeat tests carried out in our laboratory under the experimental conditions indicated in the previous section.

B. EXAFS. Recently the EXAFS theory has been re-formulated by some authors, who based their calculations on a short-range order.[6,20,21] All these theories are in quite fairly good agreement and lead to the following semiempirical relationship for the X-ray absorption coefficient:

$$\chi(k) = \frac{\mu(k) - \mu_0(k)}{\mu_0(k)} = \frac{m}{4\pi h^2 k} \sum_j \frac{N_j}{r_j^2} t_j(2k) e^{-r/\gamma(E)} \sin[2kr_j + \delta_j(k)] e^{-2k^2\sigma_j^2} \quad (11)$$

where $\mu(k)$ is the linear total absorption coefficient for a given atom, $\mu_0(k)$ is the absorption coefficient of the same structureless atom, k is the photoelectron wave vector, N_j is the number of atoms in the jth coordination shell, r_j is the averaged radial distance to the jth atom(s), $t_j(2k)$ is

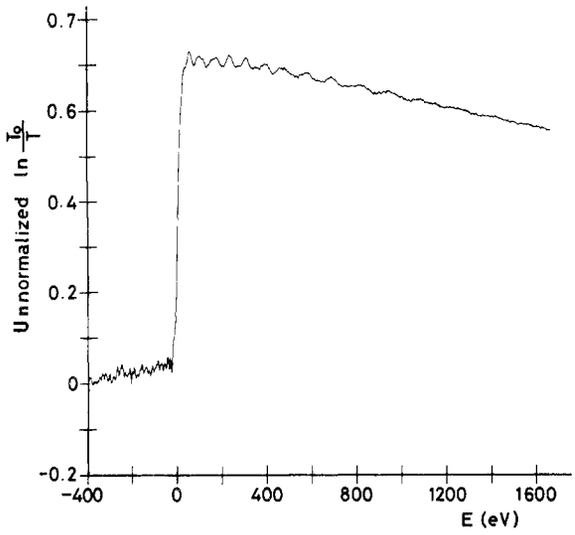

Figure 4. X-ray absorption spectrum of metallic gold. On the ordinates the absorption $\mu_x = \ln (T/T_0)$ is reported corrected for the absorption background below the edge; whereas on the abscissas the energy of the ejected photoelectrons is reported, E(eV) assuming as zero point the energy of the L_{III} absorption edge of gold.

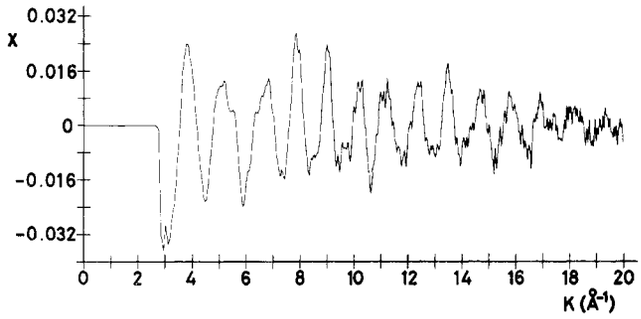

Figure 5. Normalized X-ray absorption coefficient, $\chi(k)$, of metallic Au plotted vs. the photoelectron wave vector, k(Å^{-1}).

the back-scattering matrix element encountered by the photoelectrons, $\gamma(E)$ is the mean free path of the photoelectrons, $\delta_j(k)$ is a phase shift depending on the nature of both the absorber and back-scatterer, and σ_j is the mean square root fluctuation of the atoms about their equilibrium position r_j. A decrease in temperature has the effect of sharpening EXAFS because of the σ_j term.[7] The total result is clearly a summation over all the coordination shells within the range of the effect.

Experimentally one obtains $\mu(k)$ from a plot of the sample thickness t vs. X-ray intensity by using the Lambert–Beer equation

$$\mu t = \ln \frac{I_0}{I} = \ln \frac{T}{T_0}$$

where I_0 is the intensity of the primary beam, I is the transmitted intensity; and T_0 and T are the times of collection if the preset-count technique is employed. Figure 4 reports the L_{III} EXAFS signal of metallic Au corrected from background absorption according to a Victoreen formula of the form:[22]

$$\mu = C\lambda^3 - D\lambda^4 \qquad (12)$$

where λ is the wavelength and C and D are constants found by fitting this formula to the measured absorption curve over an energy range (~400 eV) just below the L_{III} Au edge. Values of $\chi(k)$, normalized to the same per atom basis of metallic Au as well as of Au in catalysts A1141, 4433, and 2441b are reported in Figures 5–8 as functions of k.

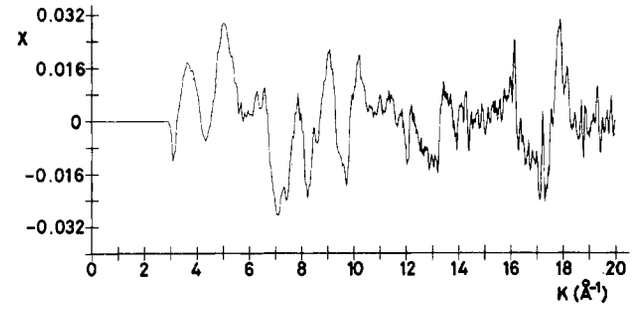

Figure 6. Normalized X-ray absorption coefficient, $\chi(k)$, of Au in catalyst A1141, plotted vs. the photoelectron wave vector k.

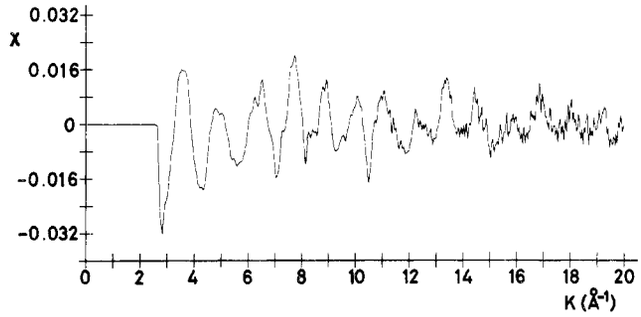

Figure 7. Normalized X-ray absorption coefficient, $\chi(k)$, of Au, in catalyst 2441b, plotted vs. the photoelectron wave vector k.

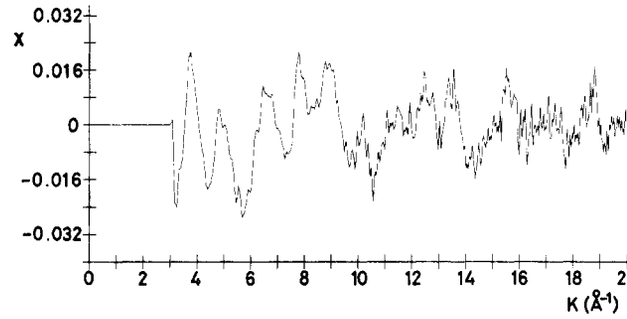

Figure 8. Normalized X-ray absorption coefficient, $\chi(k)$, of Au, in catalyst 4433, plotted vs. the photoelectron wave vector k.

Structural information can be derived from EXAFS by performing a Fourier transform.[23] This produces a radial structure function centered on the absorbing atom ($r = 0$); in this way it is possible, in principle, to obtain interatomic distances and coordination numbers.

The Fourier transform actually taken is

$$F_n(r) = \frac{1}{(2\pi)^{1/2}} \int_{k_{min}}^{k_{max}} k^n \chi(k) e^{2ikr}\, dk \qquad (13)$$

where n can be empirically chosen as 0, 1, 2, or 3, and k_{min} and k_{max} are the experimental limits.

The most serious difficulties in assigning distances are due to the presence in expression 11 of the absorption coefficient of a phase shift $\delta_j(k)$. By performing a Fourier transform, we found that the presence of a phase shift has the effect of shifting all the EXAFS peaks toward the origin by an unknown amount α. In order to recognize the true distances one must determine this value for every kind of atom surrounding the absorber by comparing the values obtained in the Fourier transform from standard compounds, whose absorber–backscatterer distances were previously determined. However, if experimental data are sufficiently accurate it is possible to determine the phase shift following a graphical method.[8] This is done for the Au metallic in Figure 9 by using the data available in Figure 5. Labeling the first maximum as zero, one obtains a value of $\alpha = 0.23$ Å from a least-squares fit of the points

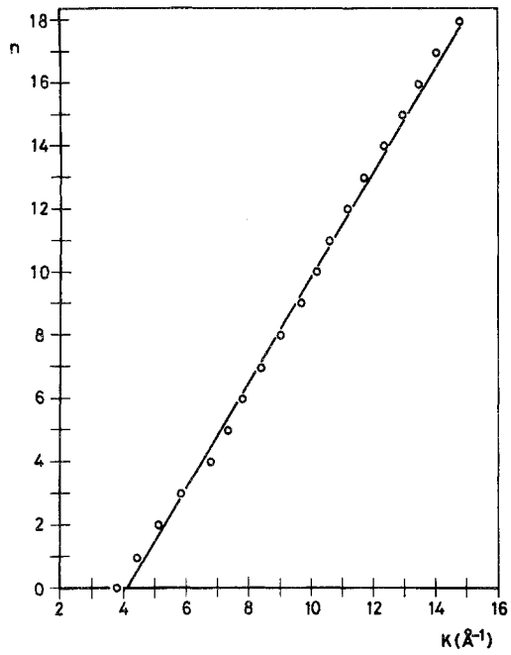

Figure 9. Plot of n vs. k for metallic Au.

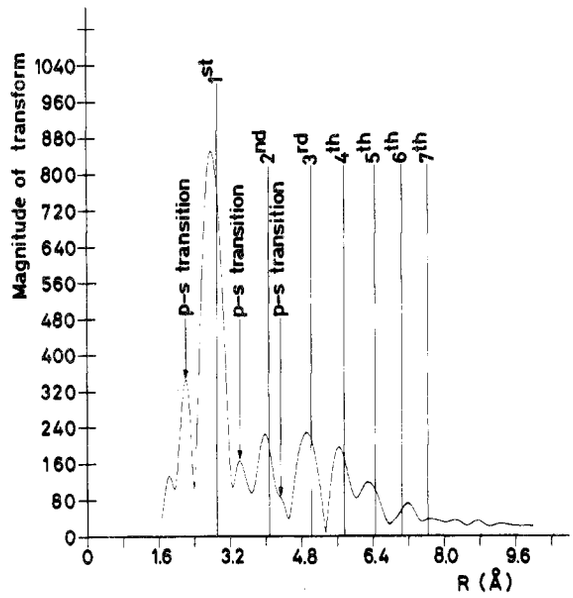

Figure 10. Magnitude of the k^3 Fourier transform of $\chi(k)$ plotted vs. radial distance from the absorbing Au atom, r', for metallic Au. The peaks corresponding to p → s transitions are indicated. The vertical lines locate on the r scale the first seven coordination shells of metallic Au, the phase shifts of the peaks corresponding to p → s and to p → d transitions are evident.

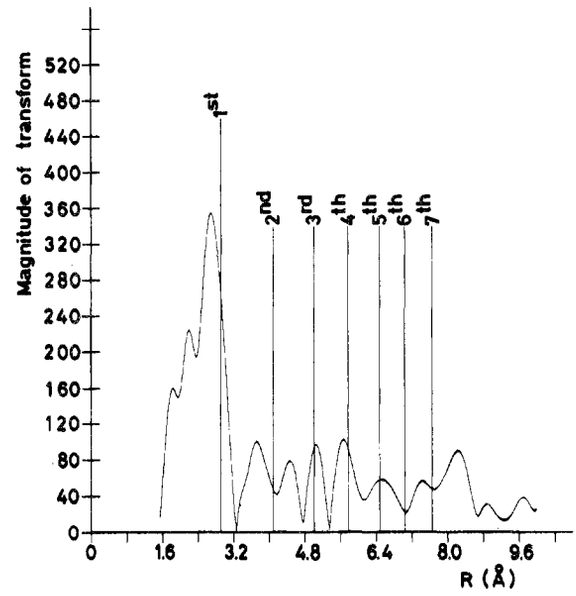

Figure 11. Magnitude of the k^3 Fourier transform of $\chi(k)$ vs. r' for catalyst A1141. The vertical lines locate, on the r scale, the first seven coordination shells of metallic Au.

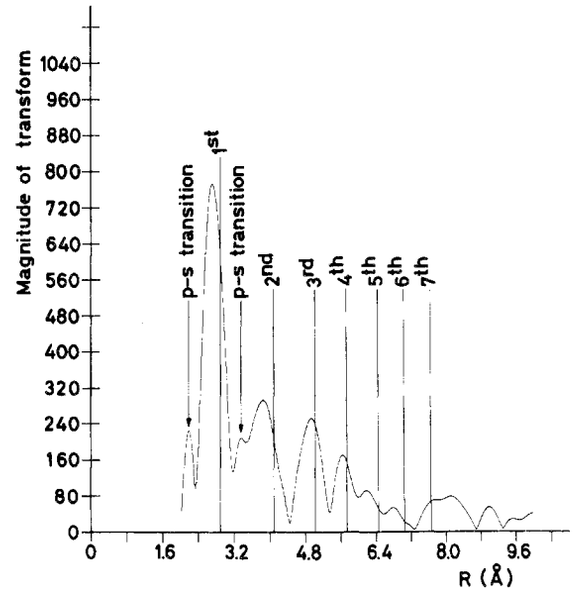

Figure 12. Magnitude of the k^3 Fourier transform of $\chi(k)$ vs. r' for catalyst 2441b, the vertical lines locate, on the r scale, the first seven coordination shells of metallic Au. The peaks due to p → s transitions are indicated.

in the plot of n vs. k, where n is an integer denoting the maxima and minima numbers of the $\chi(k)$ vs. k plot.

The magnitudes of the $n = 3$ Fourier transforms of metallic Au, as well as those of the three supported catalysts are shown in Figures 10–13. The transforms of $HAuCl_4 \cdot 3H_2O$ and Au_2O_3 are similar to those already reported.[2] All the Fourier transforms are obtained with $k_{min} = 3.5$ and $k_{max} = 14.0$ (Å^{-1}). For the first coordination shell of the standards one has[6,8,24]

$$(\mathrm{Mag}_{1s})r_{1s}^2/N_{1s} = C = \text{constant} \qquad \text{(A)}$$

where Mag_{1s} is the magnitude of the first peak of the Fourier transform of the EXAFS data for the standards, r_{1s} is its distance in Å (after correction to take into account the phase shift) from the absorbing atom, and N_{1s} is the coordination number for the first shell. Once C is defined for the standards, the coordination number, N_{1x}, for the first shell of the unknown material is given by

$$N_{1x} = (\mathrm{Mag}_x)r_{1x}^2/C \qquad \text{(B)}$$

where Mag_x and r_{1x} have the same meaning as before but are now the values defined for the unknown material.

The Debye–Waller term $e^{-2k^2\sigma_j^2}$ was considered constant since all experiments were carried out at the liquid nitrogen temperature, as already assumed by Lytle, Sayers, and Moore.[25] Structural disorder was studied following the method of Sayers, Stern, and Lytle[26] as shown in the Discussion section. Also for EXAFS experiments a precise error analysis is possible only by using several repeatibility tests. The methods employed here, as reported in the Experimental Section, are claimed to give an absolute accuracy of ±0.05 Å for the coordination distances and of ±20% for the coordination numbers.[27]

C. WAXS. Table IV reports the results obtained by wide-angle X-ray diffraction for the Au particle size,

TABLE IV: WAXS and TEM Characterization of Supported Au

catalysts	D_{WAXS},[a] Å (X-ray diffraction lines measd)	av D_{WAXS},[a] Å	c_{WAXS},[b] wt %	D_{TEM},[b] Å
A1141	(111) + (222):2800; (200) + (400):1400	2100	3.2	
4433	(111):40	40	1.9	50
2441b	(111):760; (200):380; (220):540; (311):360	500	4.2	250

[a] The precision for a related series of samples is ±10% for this parameter, while its absolute accuracy is ±25%.[28] [b] The precision of these parameters may be evaluated as ±20%.

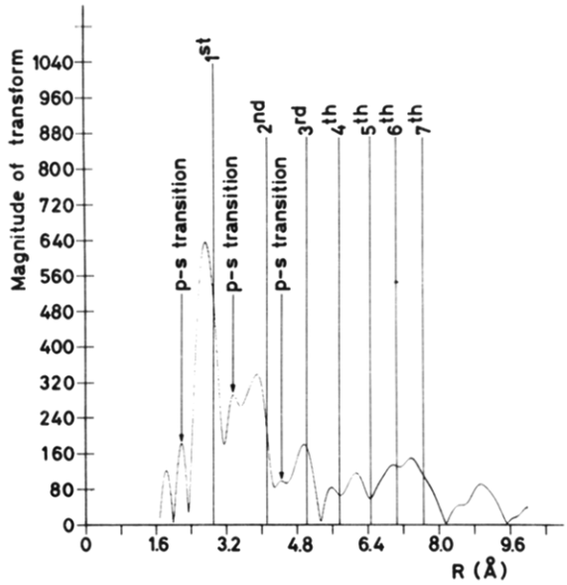

Figure 13. Magnitude of the k^3 Fourier transform of $\chi(k)$ vs. r' for catalyst 4433. The vertical lines locate, on the r scale, the first seven coordination shells of metallic Au. The peaks due to p → s transitions are indicated.

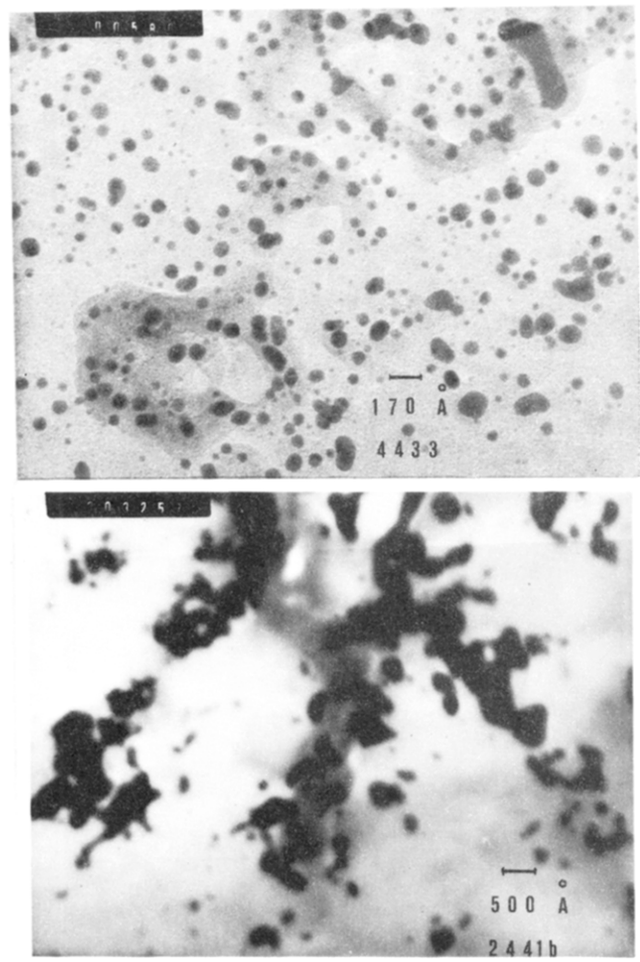

Figure 14. TEM micrographs of gold particles taken on catalysts 2441b and 4433.

determined along different crystallographic directions, and their relative averaged values. The amounts of metallic Au are reported in the fourth column of Table IV. The precision of particle size is ±10% for a related series of samples, while its absolute accuracy may be estimated as ±25%.[28] The precision for all WAXS and TEM parameters are reported in Table IV.

D. TEM. In Figure 14 are shown two microphotographs taken of catalysts 4433 and 2441b. The particle shape is approximately spherical for both samples and this fact justifies the model chosen for interpreting SAXS experimental data. Figure 15 shows the particle size distribution calculated for sample 4433 counting several hundred particles from different TEM microphotographs. The calculated average particle diameters, D_{TEM}, are reported in Table IV.

Discussion

The initial electron energy states in the L_{II} and L_{III} edges have p symmetry, and can have both s- and d-symmetric final states. In contrast with the K edges, $\chi(k)$, the L_{III} edge has two contributions, one for the final d state, χ_d, and the other for the final s state, χ_s, each weighted by its respective $\mu_L(k)$.[29] The major difference between χ_d and χ_s comes from the phase shifts δ_s and δ_d in the sine function of eq 11. This situation must be reflected in the Fourier transform of $\chi(k)$ for metallic Au as shown in Figure 10 where the theoretical position of the peaks are indicated as first shell, second shell, etc., and the peaks corresponding to p-to-s transitions are indicated as p–s transition. From the knowledge of the radial structure function of metallic Au, the values we have obtained for α_s and α_d are 0.65 and 0.11 Å. These values are slightly different from the values of 0.48 and 0.13 Å previously reported.[29] The differences may be due to the fact that while we have performed the $n = 3$ transform, the cited previous calculations[29] were made on the basis of a $n = 1$ transform. The ratio between the magnitude of the d peaks and the s peaks, as found on the Fourier transform, is about 2.5, in good agreement with the values previously[29] reported. On the basis of these findings, we estimated the effect of this situation on the $\chi(k)$ function by assuming that the ratio μ_d/μ_s may take on the same value found on the Fourier transform, between the magnitudes of the d peaks and the s peaks. The weighted average for the total α phase shift for the first shell of metallic Au must be 0.26 Å; this value is in excellent agreement with the value found by graphical means in the preceding section from the slope of the straight line of n vs. k (0.23 Å). We are aware of the fact that the absolute value of the phase shift is strongly dependent on the choice of the inner potential,[30] and that a satisfactory parametrization of the phase shift has been found for the elements from carbon to bromine,[31] that permits the definition of the interatomic distances with an accuracy of less than 0.01 Å, but little information is available for the L_{III} EXAFS data, and we wish to point

TABLE V: Theoretical, r_1, and Measured, r_1', Distances for the First Coordination Shell of the Au Reference Compounds[a]

ref compd		r_1, Å		r_1',[b] Å		α_1, Å	M	N	C
Au foil	Au-Au	2.88		2.77		0.11	851	12	588
Au_2O_3	Au-O	1.93	2.03	1.56	1.67	0.36	368	2	758
		2.12		1.77			363	2	748
$HAuCl_4 \cdot 3H_2O$	Au-Cl	2.29		1.94		0.35	518	4	679

[a] α_1 is the phase shift of the first shell; M is the amplitude of the Fourier transform peak, N is the theoretical coordination number, while $C = Mr_1^2/N$. [b] The accuracy for this parameter is ±0.05 Å.

TABLE VI: Measured, r', and Corrected, r, Distances for the First Peaks of the Supported Catalysts[a]

sample	r', Å	r, Å	Mag	N^d	N^e	atom type
A1141	1.82	2.18	160	1.1		O as Au^{3+}-O^{2-}
	2.20	2.55[b] / 2.88[c]	221	2.1		O as compound between oxygen and Au^+ / Au p → s transition
	2.70	2.81	356	4.1		Au
2441b	2.71	2.82	771	8.8	8	Au
4433	2.70	2.81	639	7.3	6	Au

[a] Mag is the amplitude of the peak as derived from the Fourier transform, N is the coordination number. [b] The value of α_d assumed for this peak is 0.35 Å as found in Au_2O_3. This value may be an overstimated value of the phase shift considering the possibility that the oxidation state of gold could be in this catalyst almost in part, +1. [c] The value α_d assumed for this peak is 0.68 Å. This value almost brings in register a part of this Fourier peak magnitude with metallic Au, considering the p to s transitions. [d] From the magnitude of the first Au-Au peak. The accuracy for this parameter is ±20%. [e] From the back-transform of the first Au-Au peak in the region $r = 2.39$, $r = 3.25$ Å.

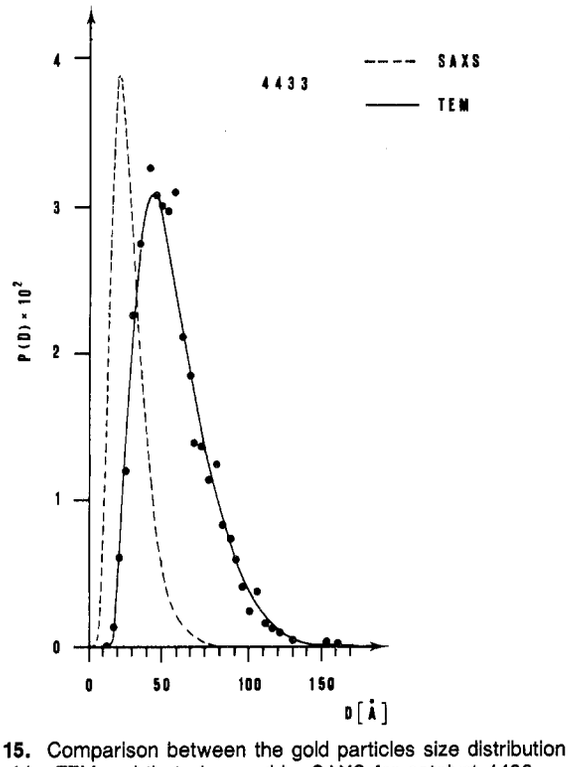

Figure 15. Comparison between the gold particles size distribution observed by TEM and that observed by SAXS for catalyst 4433.

out that our relative values of phase shifts found for the L_{III} shell of Au show very good internal consistency.

In Table V are reported the effective interatomic distances, r_1, the phase shifts, α_1, related to the first coordination sphere, the magnitude of the Fourier transform, M, the coordination number, N, and the constant, C, derived according to relationship A for the reference materials. The phase shifts values applied to the supported catalysts samples will allow us to define the nature of the chemical bonds present in the catalyst while the C constant will be used according to relation B to define the average coordination numbers related to the first coordination sphere. The results of our measurements on the catalyst samples are reported in Table VI. A constant phase shift of 0.11 Å was applied to the Au-Au distances, while a phase shift of 0.35 Å was applied to the Au-O and Au-Cl distances as found in the reference samples.

From the radial structure functions of the supported Au catalysts reported in Table VI, it is possible to conclude that the Au-Au distances are quite similar in the three samples (2.81-2.82 Å), while the shortening of the Au-Au distance in respect to the crystallographic value of 2.88 Å may be due to the fact that the α value found in metallic Au (0.11 Å) is a bit shorter than the correct value. An α value of about 0.15 Å brings all these values in register with the theoretical value.[10] Samples 4433 and 2441b show in their radial structure functions only interatomic distances interpretable with Au-Au distances. This indicates that in these two samples all the Au is present in the condensed metallic phase (particulate phase) and that no interaction detectable by EXAFS is present between Au and the support (amorphous SiO_2), notwithstanding the different dispersion shown by the two samples (see Table VII).

The radial structure function of sample A1141 is much more complicated. Before the Au-Au peak of metallic Au two weaker peaks are present, the first at $r' = 1.82$ Å and the second at $r' = 2.20$ Å. If we attribute to the first peak the phase shift found in Au_2O_3 a value of 2.18 Å is obtained which indicates the presence of Au-O bonds of the same nature as present in Au_2O_3 (Table V). The second peak with $r' = 2.20$ Å, besides resulting from the p → s transition effect, may also, almost partially, be assigned to an Au^+-O^{2-} distance. In fact from the ionic radii[32] one has $r_{Au^+} + r_{O^{2-}} = 1.37 + 1.35 = 2.72$ Å. By assuming for this Fourier peak a phase shift of 0.35 Å an interatomic distance of 2.55 Å is obtained only a little longer than the Au-O distance found in the tetrameric molecule of dimethylgold(III) hydroxide (2.40 Å).[14] The remaining part of the atomic radial structure function is much more complex and no valid assignment can be made.

We believe that the structure seen in the catalyst A1141 transform at the low r side is real and not due to noise because it corresponds, within a good approximation and after suitable corrections, to the structure already independently measured by Bassi et al.[2] on the same sample (measurements carried out at the Boeing Laboratories, Seattle, WA). According to us, this repeatibility test confirms the existence of these peaks. The only remarkable difference reported in this work for the catalyst A1141 transform with respect to the previously seen structure is a twofold ascription given to the second r peak.

TABLE VII: Average Au-Au Coordination Number as Defined on the Basis of Particle Diameters Measured by SAXS and/or WAXS[a]

catalyst	av particle diam, Å			calcd av. coordn no. of Au	M, % (EXAFS)	M, % (WAXS or SAXS)	percentage Au exposed
A1141	$D_P = 44 \pm 9$ $D_{WAXS} = 2100$	hypothesis I	$c_{SAXS} = 1.8 \pm 0.35\%$ $c_{WAXS} = 3.2\%$	10.6 ± 2	39 ± 8	72.5 ± 14	
		hypothesis II	$c_{SAXS} = 1.8\%$ $c_{WAXS} = 1.4\%$	9.9	41	46.3	15 ± 3[b]
		hypothesis III	$c_{SAXS} = 1.8\%$ $c_{WAXS} = 2.3\%$	10.3	40	59.4	
2441b	$D_P = 162$ $D_{WAXS} = 500$			10.8 11.6	81 76	94 100	10[c]
4433	$D_P = 40$ $D_{WAXS} = 40$			8.2 8.2	89 89	91 86	37[c]

[a] Percentage of total Au present in metallic phase M (%) as determined by EXAFS or directly, by WAXS, and/or SAXS methods. In the last column the percentage of Au exposed is reported. The reported error estimate may be understood for all the figures of the same column. [b] Calculated according to hypothesis III. [c] Calculated from D_P values.

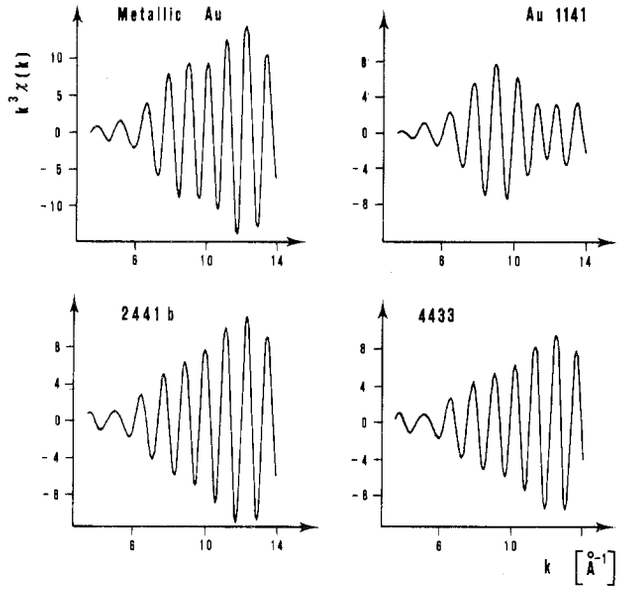

Figure 16. k space oscillations back-transformed from the first Au–Au r peak (r_1 = 2.00 Å, r_2 = 3.25 Å) for metallic gold and for the gold supported on η-Al_2O_3 (sample A1141) and on SiO_2 (samples 2441b and 4433).

In fact, in the present work, this peak is partly ascribed to a p → s transition and partly to an Au^+–O^{2-} interaction. Moreover, we have carried out a structural disorder analysis according to Sayers, Stern, and Lytle[26] with a Fourier back transform to k space of the first r peak for each supported gold sample as well as for the gold standard sample. First, we chose an interval between r_1 = 2.00 Å and r_2 = 3.25 Å and noted that the envelope of the k-space oscillation for catalyst A1141 was completely different from the other three envelopes which, on the contrary, look very similar to each other, as shown in Figure 16. This difference may be ascribed to the presence, in the above mentioned interval, of another peak which cannot be exclusively attributed to metallic gold, also taking into account the splitting due to the p → s transition. Therefore this result could be justified by the presence of the already hypothesized Au^+–O^{2-} interaction.

Proceeding with the disorder analysis, we narrowed the r interval (from r_1 = 2.39 to r_2 = 3.25 Å) for both 4433 and 2441b samples in order to eliminate the p → s transition influence in the back transform of the p → d first peak under study. The following equation was used for analyzing the new envelopes so obtained in the k space:

$$\ln \frac{\chi_{1s}(k)}{\chi_{1x}(k)} = \ln \frac{N_{1s}}{N_{1x}} + 2\Delta\sigma_1^2 k^2$$

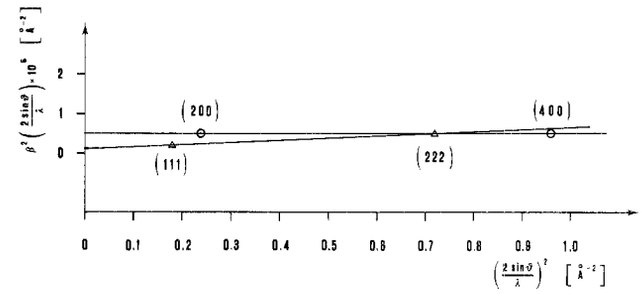

Figure 17. Plots of the integral square width $[\beta(2\sin\theta/\lambda)]^2$ vs. 4 $\sin^2\theta/\lambda^2$ for the X-ray diffraction line profiles 111–222 and 200–400, after correction for the instrumental broadening. The radiation used was Cu $K\alpha_1$ (λ = 1.5405 Å).

where $\chi_{1s}(k)$ is the EXAFS signal for the first r peak of the standard material and $\chi_{1x}(k)$ is the EXAFS signal for the first r peak of the Au catalyst examined; N_{1s} and N_{1x} are the corresponding coordination numbers and $\Delta\sigma_1$ is equal to $[\sigma_1^2(\text{metallic Au}) - \sigma_1^2(\text{catalyst})]^{1/2}$. From the plot of $\ln [\chi_{1s}(k)/\chi_{1x}(k)]$ vs. k^2 it is therefore possible to obtain the coordination number N_{1x} giving N_{1s} = 12. The following equations were obtained for samples 4433 and 2441b, respectively:

$$\ln \frac{\chi_{1s}}{\chi_1(4433)} = 0.74 + 0.00004k^2$$

$$\ln \frac{\chi_{1s}}{\chi_1(2441b)} = 0.43 + 0.00075k^2$$

The following coordination numbers were solved from these equations: N_1 = 6 for catalyst 4433 and N_1 = 8 for catalyst 2441b with an estimated error of ±20%, as reported by Hunter.[26,33] Table VI shows that the so-obtained coordination numbers are in fairly good agreement with those obtained from eq B where the magnitude of the first Au–Au peak is considered. From the slopes of the above-defined plots, the disorder results are nearly equal to zero for sample 4433 and very low ($\Delta\sigma \simeq 0.02$) for sample 2441b.

We think that such an analysis is meaningless for catalyst A1141 owing to the presence of the EXAFS Au^+–O^{2-} peak in the r space, which abundantly overlaps with the first p → d transition Au–Au peak. For this last sample we have carried out a careful analysis of the lattice disorder by means of an X-ray line broadening study on the two available couples of reflections 111-222 and 200-400 of the metallic gold lattice. For this scope the Guinier–Jagodzinski camera, equipped with a Johansson quartz monochromator for the $K_{\alpha 1-\alpha 2}$ doublet separation, was employed. From Figure 17, where the integral square

width $[\beta(2 \sin \theta/\lambda)]^2$ of the "pure" X-ray profile is plotted vs. 4 $\sin^2 \theta/\lambda^2$, it is possible to conclude that lattice imperfections are practically null for the gold phase present in this catalyst. In fact, the two straight lines so obtained are nearly parallel to the abscissa axis.[34] Moreover, the fairly good agreement among the gold concentrations determined by EXAFS, SAXS, and WAXS on all three catalysts, within the limits and the experimental errors of these techniques, is an indirect confirmation that the coordination numbers obtained neglecting disorder effects are correct. A recent paper by Friedman, Freeman, and Lytle[27] on Cu/Al_2O_3 catalysts does not consider structural disorder. Maybe such a conclusion was supported by a study similar to the present one. From the above discussion it may be concluded that in sample A1141 the supported Au is present in at least two phases: a condensed particulate phase of metallic Au, and atomically dispersed phase that interacts with the support. This conclusion is also supported by the remarkable difference existing between the Au concentration (wt %) measured by neutron activation analysis (6.9%) and the maximum Au concentration determined by X-ray diffraction methods ($c_{SAXS} + c_{WAXS} = 5.0\%$). By assuming that, at the surface of the Au particles in the particulate phase, the Au coordination number is six, and that the surface atoms may be contained in a spherical shell of 5.8 Å thickness, we found it possible to calculate, through the particle size values, the Au average coordination number for each of the catalyst samples.

This kind of averaging is necessary because the EXAFS technique averages over all the different Au atoms present in the sample. The calculated Au average coordination numbers are reported in Table VII, where different values for particle diameters determined by SAXS (Porod diameter D_P) and WAXS are indicated.

For sample A1141 where relatively large particles, beyond the SAXS experimental limit (average diameter of 2100 Å as determined by WAXS), and very small particles (average diameter of 44 Å as determined by SAXS) are present, three hypotheses may be made about the concentration of the two types of metal particles. The first hypothesis (I) is that WAXS peaks are not affected by the very small particles seen at SAXS ($c_{SAXS} + c_{WAXS} = 5.0\%$). The second hypothesis (II) considers that in the WAXS peak also an intensity contribution due to the small particles fraction is present ($c_{SAXS} + c_{WAXS} = 3.2\%$). The third hypothesis (III), which seems to us the most realistic one, is intermediate between hypotheses I and II. It considers that one-half of the contribution to the intensity of WAXS peaks, because of the small Au particles measured at SAXS, is lost in the tails of these relatively narrow peaks measured at high angle ($c_{SAXS} + c_{WAXS} = 4.1\%$).

The amount of metallic Au present in the catalyst samples, in the particulate phase, can be derived by the simple relationship:

wt % of metallic Au =
[Au–Au coordination no. found (Table VI)]/
Au–Au coordination no. calcd from appropriate particle size (Table VII)

The results of these determinations are reported in the fourth column of Table VII. Table VII contains also the weight percent of metallic Au present in the catalysts as defined by X-ray diffraction methods (either WAXS and/or SAXS methods). The agreement between the results, including hypothesis III for A1141, independently obtained by EXAFS and by X-ray diffraction is fairly satisfactory. The last column of Table VII reports the percentage Au exposed calculated as the ratio between the number of atoms present in a monolayer at the Au particles surface and the number of atoms present in the whole spherically averaged particle volume. This parameter is indicated for sample A1141 (hypothesis III), sample 2441b (referred to D_P values), and sample 4433 (referred also to D_P values).

TABLE VIII: Chemical Shifts of the Au L_{III} Absorption Edge, E, for Reference Materials and Supported Catalysts

samples	E, eV	samples	E, eV
Au	0 ± 1	A1141	−2.5
$HAuCl_4 \cdot 3H_2O$	−3.0	4433	−0.6
Au_2O_3	−3.4	2441b	−2.1

TABLE IX: Chemical Valence, z, Coordination Number, f, and Electronegativity and Effective Coordination Charge, η, for Au Preparations

sample	ion	z	electronegativity (eV/2.8)	f	η
Au_2O_3	Au^{3+}	3	1.8	4	+1.06
	O^{2-}	2	3.5		
$HAuCl_4 \cdot 3H_2O$	Au^{3+}	3	1.8	4	−0.07
	Cl^-	1	2.83		
A1141	Au^{3+}	3	1.8	6	+0.09
	O^{2-}	2	3.5		
	Au^+	1	1.42	6	−1.03
	O^{2-}	2	3.5		

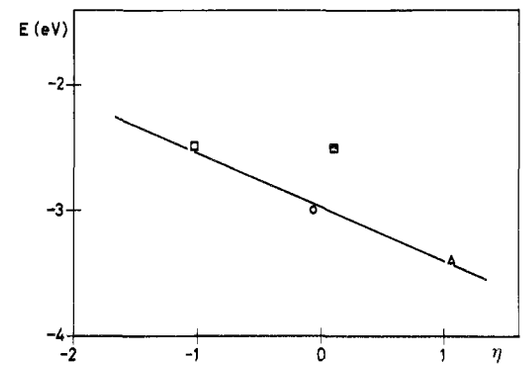

Figure 18. Effective coordination charge, η, and chemical shift, E, for the L_{III} absorption edges in sample A1141 and Au compounds: (□) sample A1141 (as Au^+); (■) sample A1141 (as Au^{3+}); (○) $HAuCl_4 \cdot 3H_2O$; (△) Au_2O_3.

If we closely examine the nature of the Au atomically dispersed phase in sample A1141, it is realized that the peak of about 2.18 Å is appropriate for Au atoms in an octahedral environment of oxygen atoms, i.e., that Au replaces Al in the Al_2O_3 lattice. The observed values of the L_{III} edge shifts are reported in Table VIII. The large experimental error and the complex coordination of the samples make a quantitative interpretation of the shifts impossible. The interesting and yet unexplained result is their negative value. Despite this, it is tempting to relate the difference in chemical shift to the binding with the support. To enlighten this point we have computed the charge that appears at the periphery of an absorbing atom of valence z as a result of being chemically bond to f near-neighbor atoms by means of a chemical bond of covalence l. This charge, the so-called effective coordination charge, η, is given by $\eta = z - fl$;[35] l was calculated from the expression $l = 1 - i$ where i is given by[32]

$$i = 1 - \exp[-\tfrac{1}{4}(X_A - X_B)^2]$$

where X_A and X_B are the electronegativities of the atoms. We have carried out the calculations for Au_2O_3, $HAuCl_4 \cdot 3H_2O$, and catalyst A1141. The results of these calculations are reported in Table IX. Using the values of

TABLE X: Rate Constant for Reaction 14 (200 °C), k_D', Activation Energy for Reaction 14, E_D, Conversion for Reaction 15, α_{NO} (350 °C), Rate of Reaction 15, v_{NO} (350 °C), and Selectivity to N_2 for Reaction 15 (350 °C), S_N[a]

catalyst	k_D', [molecules/ Au(s) s]	E_D, kcal/mol	α_{NO}, %	v_{NO}, [molecules/ A_s s] × 10^3	S_N, %
A1141		9.8	3.6	3.0	67.1
4433	2.8	12.4	15.4	1.3	14.3
2441b	4.3	9.2	5.9	6.3	21.8

[a] The error may be estimated equal to ±5% for all the quantities here reported.

L_{III} absorption edge shifts, E, given in Table VIII, we report the correlation between the effective coordination charge, η, and the edge shifts, E, in Figure 18. Considering the semiempirical character of the correlation and the experimental error in the quantitative determination of the edge shift, we obtained a fairly linear relationship. A smooth correlation has been reported between η and the L_{III} absorption salts.[36] Interestingly for sample A1141, the correlation points to Au^+ as the most likely charge state of Au atomically dispersed in the Al_2O_3 matrix.

Catalytic Activity. The catalytic activity of preparations A1141, 2441b, and 4433 has been recently investigated.[1] The study has covered measurements of the rate of the isotopic equilibration reaction

$$H_2(g) + D_2(g) \rightarrow 2HD(g) \quad (14)$$

and the selectivity in the reduction of NO by H_2:

$$2NO + 5H_2 \rightarrow 2NH_3 + 2H_2O \quad (15a)$$

$$2NO + 2H_2 \rightarrow 2H_2O + N_2 \quad (15b)$$

Reactions 14 and 15 have been studied in a flow system at a total pressure of 1 atm; for reaction 14 the temperature was 150–300 °C, H_2 partial pressure $10 < p_{H_2} < 100$ torr, and $p_{H_2}/p_{D_2} = 1$. For reactions 15 the temperature was 350 °C, $1.52 < p_{NO} < 12.16$ torr, and $6.08 < p_{H_2} < 9.12$ torr. Further experimental details may be found elsewhere.[1] The rate coefficient for reaction 14, k_D', was calculated according to the expression

$$k_D' = \frac{V}{RTA_s}\beta_\infty \ln \frac{1}{1-\alpha}\left[\frac{\text{molecules}}{\text{Au(s) atm s}}\right] \quad (16)$$

where V, R, T, and A_s are the flow rate, the gas constant, the temperature at which V has been measured, and the number of surface Au atoms per gram of catalyst, respectively, $\beta = p_{HD}/(p_{H_2})_0$, and the conversion $\alpha = \beta_t - \beta_0/(\beta_\infty - \beta_0)$, where the suffixes t, 0, ∞ refer to time t, initial time, and infinite time. According to the derivation of eq 16, k_D' may in principle be a function of p_{H_2}. However, for the three catalysts tested, k_D' was found to be independent of p_{H_2}; it is therefore numerically similar to the reaction rate constant. The rate of reaction 15, $V_{NO} = F[(NO)_o - (NO)_f]/(A_s \times 100)$ [molecules/Au(s) s], the reaction conversion, $\alpha_{NO} = [(NO)_o - (NO)_f/(NO)_o] \times 100$, and the selectivity to N_2, $S_N = 2V_N/(2V_N + V_{NH_3})$, were determined for all three samples.[1] F is the total molar flow rate, and $(NO)_o$ and $(NO)_f$ are the volume percents of NO at the reactor inlet and outlet, respectively. V_N and V_{NH_3} are the rates of formation of N_2 and NH_3, respectively. They are defined by the equations $V_N = F(N_2)_f/(A_s \times 100)$ and $V_{NH_3} = F(NH_3)_f/(A_s \times 100)$. The values obtained for k_D', the activation energy of reaction 14, E_D, α_{NO}, V_{NO}, and S_n are reported in Table X.

Gold supported on Al_2O_3 was found more selective toward N_2 formation than gold supported on SiO_2. It was suggested than an associative chemisorption of NO is responsible for NH_3 formation whereas a dissociative NO chemisorption is the precursor for N_2.[1] The relative amount of the two chemisorption states was related to more or less oxidized gold sites. A more reduce site increases, by back-donation, the electron density into the π^* antibonding orbital of the NO molecule, inducing a destabilization and bond weakening in the NO adsorbate (dissociative chemisorption). The role of the support in modifying the reactivity and selectivity of Au was related to the support tendency to donate or accept electrons. Therefore, it was proposed gold sites on SiO_2 are more electron deficient than on Au–Al_2O_3 samples. Supporting evidence for this interpretation on the nature of the metal–support intersection may be found in the more severe conditions required to produce reduced gold on SiO_2 than on Al_2O_3.[37]

The results of the extensive morphological and structural study reported in this paper show that, according to the lower amount of Au exposed in both catalysts A1141 and 2441b with respect to Au exposed in catalyst 4433, the catalytic activity of the first two samples is clearly lower than that of catalyst 4433. On the other hand, the selectivity found in NO reduction by H_2 for catalyst A1141 supported on η-Al_2O_3 is much higher than that found for catalysts 4433 and 2441b supported on SiO_2. These findings confirm the idea that the interaction between Au and the support has an electronic nature. We believe that this interaction is a key factor in determining the electronic density on the gold active site.

It is worth noting that EXAFS has been the only technique (among those employed in the characterization) able to detect the presence of different gold species between Au–SiO_2 and Au–Al_2O_3 preparations. Unfortunately, at this stage, EXAFS data on the oxidation state of Au do not give precise information because of several reasons:

(a) The correlation between the L_{III} shift and the oxidation state is not well understood and needs to be further investigated.

(b) The values of the L_{III} shift have been measured at temperatures, pressures, and gas phase compositions, very different from the reaction conditions.

(c) The results obtained are an average value for the total atoms of Au, while from a catalytic point of view we are interested in the Au atoms that are active sites for the reaction.

Acknowledgment. The work was carried out with the partial financial support of the National Science Foundation (U.S.A.) and C.N.R. (Italy). This support is gratefully acknowledged.

References and Notes

(1) S. Galvagno and G. Parravano, in press.
(2) I. W. Bassi, F. W. Lytle, and G. Parravano, *J. Catal.*, **42**, 139 (1976).
(3) J. W. Anderegg, P. G. Mardon, and R. W. Hendricks in "An Alignment Procedure for the Kratky Small Angle X-ray Camera", Report ORN6-4476, Oak Ridge National Laboratory, Oak Ridge, Tenn., 1970.
(4) T. E. Whyte, Jr., P. W. Kirklin, R. W. Gould, and H. Heinemann, *J. Catal.*, **25**, 407 (1972).
(5) O. Kratky, I. Pilz, and P. J. Schmitz, *J. Colloid Interface Sci.*, **21**, 24 (1966).
(6) E. A. Stern, *Phys. Rev. B*, **10**, 3027 (1974).
(7) G. Beni and P. M. Platzman, *Phys. Rev. B*, **14**, 1514 (1976).

(8) F. W. Lytle, D. E. Sayers, and E. A. Stern, *Phys. Rev. B*, **11**, 4825 (1975).
(9) J. A. Bearden, *Rev. Mod. Phys.*, **39**, 78 (1967).
(10) J. A. Bearden and A. F. Burr, *Rev. Mod. Phys.*, **39**, 125 (1967).
(11) E. G. Hofman and H. Jagodzinski, *Z. Metallk.*, **46**, 601 (1955).
(12) O. Mueller, R. E. Newnham, and R. Ray, *J. Inorg. Nucl. Chem.*, **31**, 2966 (1969).
(13) H. D. Wasel-Nielen and R. Hoppe, *Z. Anorg. Allg. Chem.*, **359**, 36 (1968).
(14) G. E. Glass, J. H. Konnert, M. G. Miles, D. Britton, and R. S. Tobias, *J. Am. Chem. Soc.*, **90**, 1131 (1968).
(15) A. Guinier and G. Fournet, "Small-Angle Scattering of X-Rays", Wiley, New York, 1955, pp 126–135.
(16) R. Baur and V. Gerold, *Acta Metall.*, **12**, 1149 (1964).
(17) G. Fagherazzi, G. Cocco, L. Schiffini, S. Enzo, A. Benedetti, R. Passerini, and G. R. Tauszik, *Chim. Ind. (Milan)*, **60**, 892 (1978).
(18) O. Kratky, "Proceeding of the Interdisciplinary Conference on Electromagnetic Scattering", Pergamon Press, Oxford, 1963, pp 459–476.
(19) S. R. Sashital, J. B. Cohen, R. L. Burwell, Jr., and J. B. Butt, *J. Catal.*, **50**, 479 (1977).
(20) C. A. Ashley and S. Doniach, *Phys. Rev. B*, **11**, 1279 (1975).
(21) P. A. Lee and J. P. Pendry, *Phys. Rev. B*, **11**, 2795 (1975).
(22) "International Tables for X-ray Crystallography", Vol. III, K. Lonsdale et al., Ed., Kynoch, Birmingham, England, 1962, Section 3.2, p 161.
(23) D. E. Sayers, E. A. Stern, and F. W. Lytle, *Phys. Rev. Lett.*, **27**, 1204 (1971).
(24) E. A. Stern, D. E. Sayers, and F. W. Lytle, *Phys. Rev. B*, **11**, 4825 (1975).
(25) F. W. Lytle, D. E. Sayers, and E. B. Moore, *Appl. Phys. Lett.*, **24**, 45 (1974).
(26) D. E. Sayers, E. A. Stern, and F. W. Lytle, *Phys. Rev. Lett.*, **35**, 584 (1975).
(27) R. M. Friedman, J. J. Freeman, and F. W. Lytle, *J. Catal.*, **55**, 10 (1978).
(28) R. C. Grovie, *J. Phys. Chem.*, **69**, 1238 (1965).
(29) F. W. Lytle, D. E. Sayers, and E. A. Stern, *Phys. Rev. B*, **15**, 2426 (1977).
(30) P. A. Lee and G. Beni, *Phys. Rev. B*, **15**, 2862 (1977).
(31) P. A. Lee, B.-K. Teo, and A. L. Simons, *J. Am. Chem. Soc.*, **99**, 3856 (1977).
(32) L. Pauling, "The Nature of Chemical Bond", Cornell University Press, Ithaca, N.Y., 1948.
(33) S. H. Hunter, Stanford University SSRP Report No. 77/04, March 1977.
(34) G. Fagherazzi and G. Lanzavecchia, *Mater. Sci. Eng.*, **5**, 63 (1970).
(35) S. S. Batsanov, "Electronegativity of Elements and Chemical Bonds", USSR Academy of Science Publishers, Novosibirsk, 1962.
(36) I. A. Ovsygannikova, S. S. Batsanov, L. I. Nasonova, L. R. Batsanova, and E. A. Nakrasov, *Acad. Sci. USSR, Phys. Ser.*, **31**, 936 (1967).
(37) G. C. Bond and P. A. Serman, *Gold Bull.*, **6**, 102 (1973).

Quantum Chemical Study of the Electronic Structure of Na–X and Na–Y Zeolites

S. Beran* and J. Dubský

The J. Heyrovský Institute of Physical Chemistry and Electrochemistry, Czechoslovak Academy of Sciences, 121 38 Prague 2, Máchova 7, Czechoslovakia *(Received November 3, 1978; Revised Manuscript Received April 9, 1979)*

Models were proposed for the Na–X and Na–Y zeolites with four clusters containing up to 37 atoms. The electronic structure of this model was studied by the CNDO/2 method. Charge densities on individual atoms forming the zeolite skeleton for various Si:Al ratios were calculated. The type of coordination of the Na atom in the zeolite skeleton and the character of the bonding of the Na atoms in the skeleton were also studied.

Introduction

In recent years a number of authors have carried out theoretical studies of the electronic structures of various types of aluminosilicates and the interactions of atoms or molecules with active sites in model clusters.[1-8] The ever increasing importance of zeolites in many branches of catalysis and especially their possible use (particularly of the new type ZSM) for the synthesis of higher hydrocarbons from various oxygen-containing organic compounds has led to the development of quantum chemical calculations in this area.

This work was carried out in order to obtain data on the electronic structure of zeolites of the faujasite type (Na–X or Na–Y), particularly on the magnitude of the charge on individual types of atoms in the zeolite cluster, which are necessary for calculation of the physical interactions of molecules with zeolites[9-11] and for calculation of the electrostatic field of zeolites.[12] A good deal of attention has also been devoted to study of the manner in which Na^+ ions are coordinated in the zeolite skeleton, i.e., to determine the character of Na atoms–zeolite skeleton bonds, and to clarify the differences in the individual positions in which the Na^+ ion can be coordinated. The effect of the Si:Al ratio on these characteristics has also been studied.

Models and Methods

The present state of quantum chemical methods and computation technique does not give the possibility of calculating systems containing several hundred atomic orbitals. Consequently, it was not possible to use the unit cell for modeling zeolite or even to study a single cubooctahedron; we were thus forced to work with zeolite clusters which were much smaller. Figure 1 depicts the model which we used for zeolites of the faujasite type (clusters A, B, C, and D), which considers all the planes of the cubooctahedron and prisms. More detailed description of these cluster with indication of the individual types of atoms and their numbering can be seen in Figures 2–5. Zeolite continuation (i.e., cluster termination) was realized through hydrogen atoms, which is the usual method employed in forming models for infinite systems by the cluster technique.[2-8,13,14] Simultaneously, however, these groups represent a model of surface hydroxyl groups which terminate the actual zeolite crystal. The cluster geometry used in the calculations was found from the data in ref 15; i.e., the Si–O and Al–O bond lengths are taken equal for all Si:Al ratios assumed. Having distorted the zeolite clusters so that the Si–O bond lengths were shortened and the Al–O bond lengths were simultaneously extended by 0.1×10^{-10} m (compared with identical Si–O and Al–O bond lengths[15]), we have found the calculated changes of the charges on atoms negligibly small. This fact justifies the use of the rigid cluster geometry. The length of the O–H bonds of the terminal hydroxyl groups –X–O–H (X is a Si or Al atom; the X–O–H atoms lie on a straight line) was kept constant, 1.08×10^{-10} m.

Clusters A and B. containing six X atoms, were studied for the case when the Si:Al ratio has values of ∞, 5, 2, and 1. For a Si:Al ratio of 2, two positions of Al atoms located on the sixfold zeolite window were studied: (i) the Al atoms are separated by one Si atom; (ii) the Al atoms are

0022-3654/79/2083-2538$01.00/0